Journal of Volcanology and Geothermal Research 466 (2025) 108396

Contents lists available at ScienceDirect

Journal of Volcanology and Geothermal Research

journal homepage: www.journals.elsevier.com/journal-of-volcanology-and-geothermal-research

Heat from dyke intrusions released by boiling of warm groundwater and steaming into the atmosphere during the 1975–1984 eruptive and intrusive activity at Krafla, Iceland

Patricia Fehrentz [a,*], Magnús T. Gudmundsson [a], Hannah I. Reynolds [a], Anette K. Mortensen [b], Sydney R. Gunnarson [c], Joaquin M.C. Belart [c], Michaela A. Chodora [d]

[a] Institute of Earth Sciences, University of Iceland, Sturlugata 7, 102 Reykjavík, Iceland
[b] Landsvirkjun (National Power Company of Iceland), Katrínartúni 2, 105 Reykjavík, Iceland
[c] Náttúrufræðistofnun (Natural Science Institute of Iceland), Smiðjuvöllum 28, 300 Akranes, Iceland
[d] Neotectonics and Natural Hazards Group, RWTH Aachen, Lochnerstraße 4-20, 52056 Aachen, Germany

ARTICLE INFO

Keywords:
Geothermal areas
Heat budget
Steam clouds
Dyking

ABSTRACT

The Krafla volcano-tectonic episode in NE-Iceland in 1975–1984 was associated with approximately 10 m widening of the plate boundary within the Krafla caldera, where a high-temperature geothermal system is located. A composite dyke was formed, with an estimated volume 0.15–0.31 km^3 within the geothermal reservoir, releasing thermal energy of 0.5–1.0 × 10^{18} J. An empirical relation between the area of steam clouds in air photos and their heat output was used to assess heat loss to the atmosphere by steaming during the Krafla fires. The applicability of this method for Krafla was tested in 2024 at selected locations where steam flow could be measured directly. Analyses of vertical air photos obtained several times in 1976–1985, notably during and after the eruptive events, show that steaming was mainly prevalent in the vicinity of the eruptive fissures. The heat loss to the atmosphere within the geothermal area was ~0.9 MW/m during eruptions, declining to a more long-term value (~0.05 MW/m) in 50–100 days. This enhanced steaming after the dyke injection/ eruption is considered to be caused by the interaction of the groundwater/shallow geothermal fluid with the uppermost 110–400 m of the dyke and appears to account for about one-third of the total heat lost in this way to the atmosphere. The remaining two-thirds were lost gradually throughout the rifting episode. The heat lost to the atmosphere (~5–10 % of the total energy) was an order of magnitude smaller than the 90–95 % of the thermal energy added to the geothermal reservoir by the dyke.

1. Introduction

Iceland has several young igneous geothermal systems, deriving their heat from magmatic intrusions in the crust. The high occurrence of young igneous systems is due to the high magma production rate, as Iceland sits on the Mid-Atlantic Ridge and is underlain by a mantle plume. Bodvarsson (1982) estimated the rate of heat flow in Iceland as 30 GW, whereof advection and convection of geothermal water accounts for 8.5 GW: 8 GW at high-temperature areas and 0.5 GW at low-temperature systems. Iceland contributes 8.5 % of the global subaerial heat losses by hydrothermal processes (Bodvarsson, 1982).

For young igneous geothermal systems, magma intruded into the roots is considered to be the main source of heat (e.g. Stimac et al., 2015). Intrusive and eruptive events provide heat into the geothermal system, as cooling and solidification of the magma heats the surrounding host rock and groundwater in the porous matrix. Heating and evaporation of the water leads to convection and steam may rise up through fissures. As it reaches the surface, the steam diffuses into the atmosphere. The heat lost by steam released into the atmosphere can be a significant parameter when determining the heat budget of a geothermal system. However, the importance of steaming, in association with dyking, on the heat budget of young igneous systems has not received much attention.

Hochstein and Bromley (2001) determined heat flow by steaming into the atmosphere at the Karapiti geothermal field in New Zealand by comparing the size of steam clouds rising from fumaroles, with the

* Corresponding author.
E-mail address: paf6@hi.is (P. Fehrentz).

https://doi.org/10.1016/j.jvolgeores.2025.108396
Received 4 April 2025; Received in revised form 8 June 2025; Accepted 9 June 2025
Available online 10 June 2025

measured mass flux of steam creating the clouds. This study from New Zealand is analogous to the one used here, where the acquisition of vertical aerial photographs was carried out several times during the major rifting and eruptive episode of the Krafla volcanic system in north Iceland in 1975–1984. Moreover, the applicability of the Hochstein-Bromley approach is tested for the Bjarnarflag area to the south of the main Krafla geothermal area, using steam cloud observations at a power plant where the mass fluxes of steam and hence the energy fluxes were also measured (see subsection 3.2).

Fridriksson et al. (2006) and Oddsson (2016) determined heat flux in Icelandic geothermal areas, including heat loss by fumaroles estimated by calorimetry. Moreover, the conditions at ice-covered volcanoes and geothermal systems provide opportunities to do relatively precise calorimetric estimates of the heat output of the geothermal system by ice surface mapping, including those associated with the central volcanoes of Grímsvötn (Bjornsson and Gudmundsson, 1993; Reynolds et al., 2018), Bárðarbunga (Reynolds et al., 2019) and Katla (Jarosch et al., 2023).

The Krafla volcano in NE Iceland is one of the best-studied volcanoes, and its high-enthalpy geothermal system is utilized for energy production. The so called "Krafla fires" refer to its most recent episode of volcanic activity and rifting from 1975 to 1984. It was a series of 20 dyke events from which 9 reached the surface and lead to an eruption (e.g. Einarsson and Brandsdottir, 2021). This rifting episode is well documented by, for example, geodetic and seismic measurements (e.g. Einarsson and Brandsdottir, 2021; Tryggvason, 1984). The results obtained from these studies constrain the amount of spreading and the volume of intrusions formed. Analysis of aerial photographs that were taken repeatedly during the Krafla fires, makes it possible to estimate the size of steam plumes formed by boiling of shallow geothermal fluid and groundwater extracting heat from the dyke formed. The heat loss to the atmosphere through steaming is quantified using the empirical relationship of Hochstein and Bromley (2001). By comparing energy lost by the geothermal system during the period of volcanic activity to the energy injected by dyking, we can estimate how much of the energy released remains in the geothermal system.

2. Geological setting

Krafla is one of the central volcanoes in the Northern Volcanic Zone of Iceland. It forms the center of a 100 km long volcanic system, trending N 10°E, extending from about 40 km south and 60 km north from the center of the 10 km (E-W) by 8 km (N-S) Krafla caldera (e.g. Hjartardottir et al., 2012). The caldera is about one hundred thousand years old and extensively filled by the deposits of post-collapse volcanism. The size of the geothermal system within Krafla is constrained by information from drillholes and TEM soundings (e.g. Mortensen et al., 2015). Its width (north-south) is approximately 6 km, extending from the southern margin of the caldera to 1 km south of the northern margin. Fig. 1 shows the extent of the high resistivity core at 600 m depth (Árnason and Magnússon, 2001), indicating the high-temperature geothermal system (Mortensen et al., 2015; Arnason et al., 2000).

The Krafla volcanic system has had several periods of volcanic activity throughout the Holocene (Sæmundsson, 1991), with the latest being the Mývatn fires in 1725–1729 and the Krafla fires in 1975–1984. These unrest events were both associated with widening of the fissure swarm, fissure opening, dyke formation and lava effusion on the surface (Sæmundsson, 1991). The Krafla area has been extensively studied in relation to the Krafla fires of 1975–1984 and its geothermal exploitation (e.g. Arnason, 2020; Einarsson and Brandsdottir, 2021; Tryggvason, 1984). The occurrence of geothermal surface manifestations around Krafla volcano are shown in Fig. 1. Active areas are presently found at three locations (e.g. Sæmundsson, 1991):

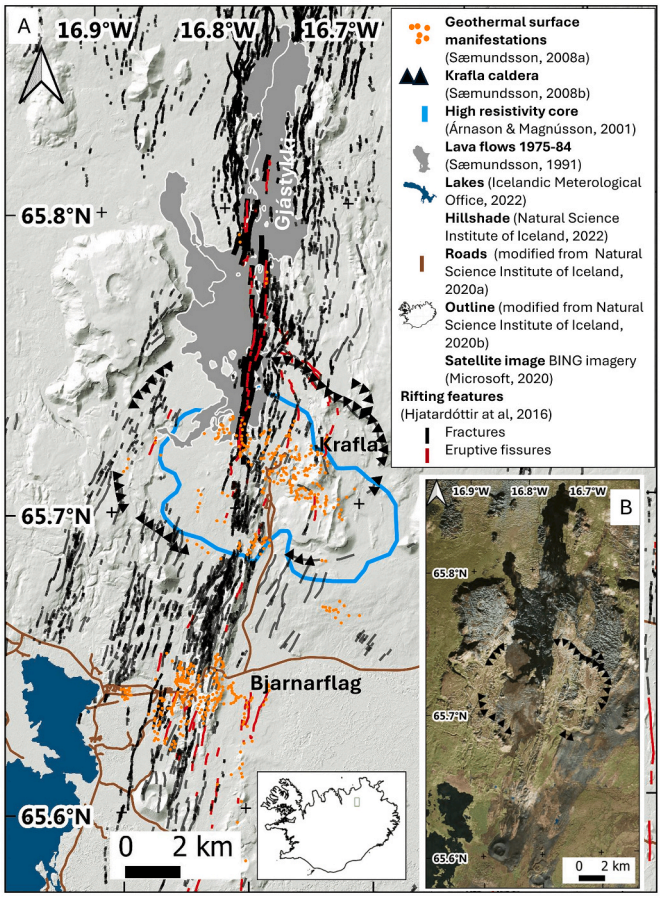

Fig. 1. Geological setting of the Krafla volcano showing faults, geothermal manifestations, the location of the Krafla caldera and its high-resistivity core at 600 m depth (Árnason and Magnússon, 2001; Hjartardóttir et al., 2016; Natural Science Institute of Iceland, 2020a; Natural Science Institute of Iceland, 2020b; Natural Science Institute of Iceland, 2022; Icelandic Meteorological Office, 2022; Microsoft, 2022; Sæmundsson, 1991; Sæmundsson, 2008a; Sæmundsson, 2008b).

1. The Krafla caldera, where the main system is located, has visible surface activity covering about 10 km^2. This area has been exploited to run the Krafla power station since the 1980s.
2. The Bjarnarflag area to the south of Krafla, where spots of vigorous fumarole activity are observed within an area of 3–4 km^2.
3. Gjástykki, a flat rift-valley/graben, located 5–10 km to the north of the northern margin of the Krafla caldera. Gjástykki has had some geothermal activity for at least centuries, while visible signs of ongoing activity were subtle in the decades prior to the Krafla fires, when, steaming increased a great deal (Sæmundsson, 1991) and is still active.

Fig. 2 shows the evolution of the area of hot ground around Krafla Mountain over the period 1977–2004. A marked decrease has occurred after the end of the Krafla fires. Fig. 3 shows schematically the main features of the Krafla geothermal system, as summarized in Scott et al. (2022). Fractures and faults trend approximately N 10°E, perpendicular to the direction of spreading, as did the fissures and the dyke injected during the Krafla fires. Fumaroles and steaming, as well as alteration, are found above the dyke and in the fissures (e.g. Arnason, 2020; Oskarsson, 1984), and as seen in the aerial photographs by National Land Survey of Iceland (National Landsurvey of Iceland (Landmælingar), 1977–1985) acquired during the unrest period. The Krafla fires (1975–84) consisted of 20 intrusive and eruptive events. The seismic activity suggests that dyking occurred over a 70 km segment of

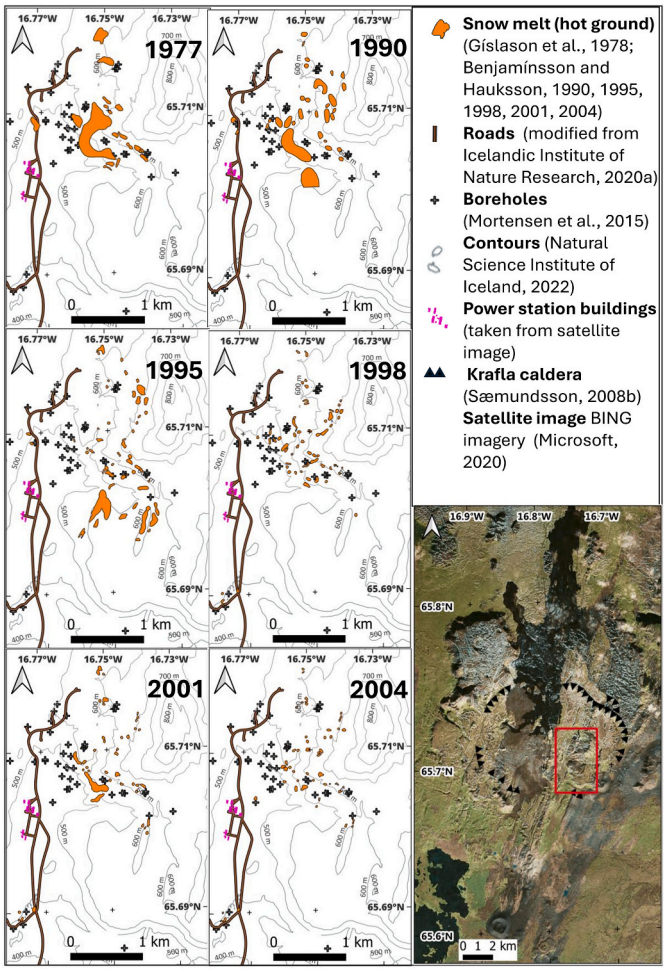

Fig. 2. Areas of snow melting between 1977 and 2004 (Benjamínsson and Hauksson, 1998; Benjamínsson and Hauksson, 2001; Benjamínsson and Hauksson, 2004; Benjamínsson and Trausti, 1990; Benjamínsson and Trausti, 1995; Gislason et al., 1978; Natural Science Institute of Icelan, 2020a; Natural Science Institute of Iceland, 2022; Microsoft, 2022; Mortensen et al., 2015; Sæmundsson, 2008b).

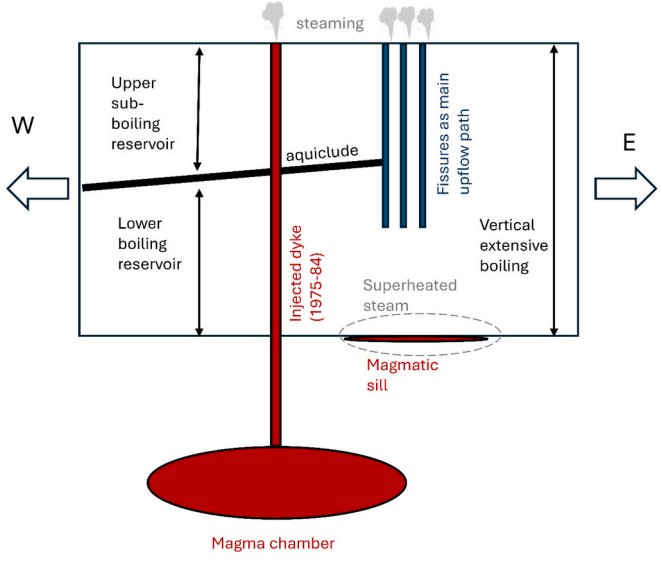

Fig. 3. Cross-sectional sketch of the Krafla geothermal system, as summarized in Scott et al. (2022).

the plate boundary, with its southern end, east of Lake Mývatn, while the northern end is located offshore, in the fjord Öxarfjörður (Einarsson and Brandsdottir, 2021). The rifting associated with the Krafla fires reached approximately 9 m within the caldera (Arnadottir et al., 1998; Hollingsworth et al., 2012; Tryggvason, 1984).

3. Methods

3.1. Thermal energy estimates of the dyke using geodetic and seismic data

Thermal energy that can be released from a magmatic intrusion (basalt in the case of the Krafla fires) to the surrounding rocks consists of the latent heat released by solidification and the sensible heat released by cooling down to the temperatures of the surroundings, in the case of Krafla, the active geothermal system:

$$E = V\rho\left(L + c_p\left(T_m - T_{sys}\right)\right) \quad (1)$$

Here V is the volume of the dyke intruded into the geothermal system, ρ and c_p are respectively the density and heat capacity of basalt, T_m is the initial magmatic temperature and T_{sys} the average temperature of the geothermal system. It is assumed that the volume of the dyke can be estimated as that of a rectangular body. We are interested in the volume of the dyke which is thermally affecting the geothermal system, see Fig. 4. Its geometrical parameters can be determined using previous research and are described further in Section 4.1 and Table 2. The horizontal extension of dykes intersecting the geothermal system is based on the seismic activity during the Krafla fires (e.g. Einarsson and Brandsdottir, 2021). The width of the dykes is based on studies of deformation and surface opening during the rifting episode (Arnadottir et al., 1998; Hollingsworth et al., 2013; Hollingsworth et al., 2012; Tryggvason, 1984). The height of the dyke used for this purpose is

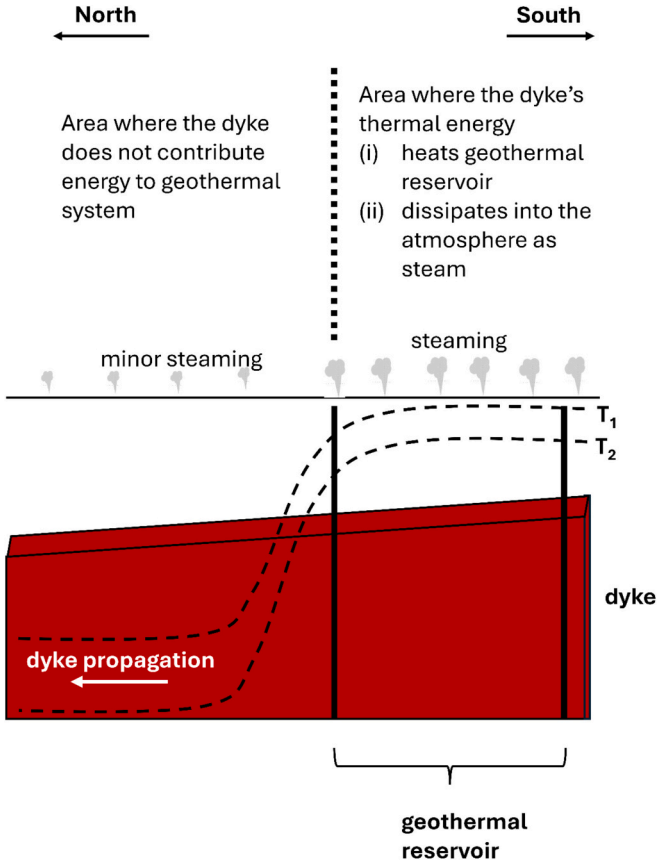

Fig. 4. Effect of dyke formation within and outside a geothermal reservoir. In this study, we only consider the dyke's energy within the geothermal reservoir.

considered to correspond to the thickness of the geothermal system. It is based on the assumed depth of convective activity (Violay et al., 2012) and the brittle-ductile transition in the caldera (Ágústsson et al., 2012).

3.2. Determining the order of magnitude heat release to the atmosphere by steaming

Hochstein and Bromley (2001) obtained data on the size of steam clouds from vertical aerial photographs of the Karapiti fumarole field in the Wairakei geothermal area in New Zealand and combined it with independent measurements of heat, based on digital pressure meters and thermistors to obtain an empirical relationship between the cloud size (area on the vertical aerial photographs) and heat output. The size of clouds in the aerial photographs varied over two orders of magnitude (8 m^2 to 780 m^2), as did the measured heat output range (0.24 MW to 18.5 MW). We used the approach of Hochstein and Bromley (2001), consisting of the following steps for the aerial photo analyses:

1. To account for variable steam content in a cloud, the opaque (A_o) and semi-opaque (A_{so}) areas were determined and the area (A) used in the calculations was defined as

$$A = A_o + 0.5 \cdot A_{so} \quad (2)$$

2. The aerial photographs used by Hochstein and Bromley (2001) were not taken on the same dates as the heat flow measurements. The values used were the time-weighted average of the area for the two dates. If aerial photographs were taken only before or after, only that value was used.
3. The results show a linear relationship between power and steam cloud area

$$P = c_1 \cdot A \quad (3)$$

With P being the power of steaming. Using the values of P and A from Table 1a and b in Hochstein and Bromley (2001) the best fit scaling factor for their data (steam cloud area and steam flow rate for selected fumaroles) is $c_1 = 2.3 \pm 0.2 \bullet 10^4\ W/m^2$.

Table 1
Aerial photographs obtained at Krafla in the period 1976–1985.

Date and time	Flight line	Flight height [m]	Time after the start of the previous eruption [days]
02-Sep-1976 11:15	Gjástykki-Krafla	4800	257
20-Aug-1977 14:53	Leirhnjúkur	2200	115
09-Sep-1977 12:09	Leirhnjúkur	1830	1
09-Jun-1980 12:51	Leirhnjúkshraun / Kröfluvirkjun-Gjástykkisbunga	3600	85
27-Jul-1980 12:18	Leirhnjúkur- Hrútafjöll	3600	17
22-Oct-1980 13:37	Leirhnjúkur- Gjástykki	6700	4
08-Feb-1981 14:28	Gjástykki	2440	9
21-Aug-1982 12:34	Þeistareykjabunga-Leirhnjúkshraun/ Gjástykki-Krafla	5486	276
22-Sep-1985 12:48	Gjástykki-Krafla/ Leirhnjúkur-Bunguvegur/ Leirhnjúkshraun-Sandfell	2350	383

Hochstein and Bromley (2001) used normalized values where area for each fumarole cloud is scaled by the total sum of steam cloud area. Since we are seeking absolute values of energy output, the aim is to use Eq. (3) to calculate the total heat released at the time of air photo acquisitions over the period of the Krafla fires.

An approximation made in these estimates is that the steam cloud area is proportional to its volume. This approximation seems to work reasonably for the empirical data (Hochstein and Bromley, 2001) and should be applicable for bodies that resemble a sphere, ellipsoid, inverted cone, etc.

3.2.1. Applicability to Icelandic geothermal systems

To test the validity of the relationship derived in Eq. (4) for the Krafla area, NE-Iceland, we did a time-lapse photography at the Bjarnarflag power plant on 9–10 July 2024, where the mass flow of steam out of the power plant, borehole BN09, and the steaming tower close to the separation station 2 was measured directly a few days earlier. The energy flux, P (the power of steaming) into the atmosphere is proportional to the mass flux ($\dot{m}$) and h, the enthalpy of the steam.

$$P = h\dot{m} \quad (4)$$

Timelapse cameras were set up at three locations close to the Bjarnarflag power plant (Fig. 5). As they had to be set up at good viewpoints, it was not possible to choose the locations for the viewpoints exactly perpendicular to each other. The first location was west of the power plant. The other location was in the southeast on the first day and the third to the southwest on the second day. Photographs, where the different steam clouds could not be reliably separated, were discarded from analysis. This situation applied over some intervals of the survey period and depended mostly on wind intensity and direction. The area of steam shown in the photographs was determined and the power of steaming and a mass flow rate calculated, using Eqs. (2) and (3). The length measured in the aerial photographs in pixels (L_p), could be converted to meters (L_m) by determining the ratio of the horizontal field of view of the camera (α_h) and the number of pixels (n) in the horizontal direction (α_h/n) and multiplying it by the distance r between the camera and the object (the steam cloud). This approximation is considered valid for all objects within a viewing angle less than 15° from the viewing direction of the camera (small angle approximation):

$$L_m = L_p \cdot (\alpha_h/n) \cdot r \quad (5)$$

The plume size (area) found from the horizontal view of the time lapse photographs is considered to be approximately the same as it would be found from a vertical view. This was tested for the photographs used in the assessments, where the observed plume width (horizontal) as seen from the camera view along the plume direction, and plume thickness (vertical) as seen from the camera with a view perpendicular to it was checked (Fig. 5). This test was done for all the 13 instances used in the area estimation. Moreover, the possible difference between plume area estimated for both, the horizontal view and vertical view, was assessed. The data indicated a ratio of vertical and horizontal area of 1.2 ± 0.2. The assumption of approximately similar vertical and horizontal area is therefore considered valid for all time-lapse-photographs that had a viewing angle oriented 90 ± 15° to the wind direction.

3.2.1.1. Effect of humidity. Fig. 6 shows the relationship between the calculated power and the relative humidity at the nearby Mývatn/Reykjahlið weather station. As the humidity values at the weather station are available once every hour, the values used for each photo were obtained as the time-weighted average of the hourly observation before and after. The mass flow is assumed to be constant, but varying humidity influences the diffusion of the steam; when humidity is lower, the steam

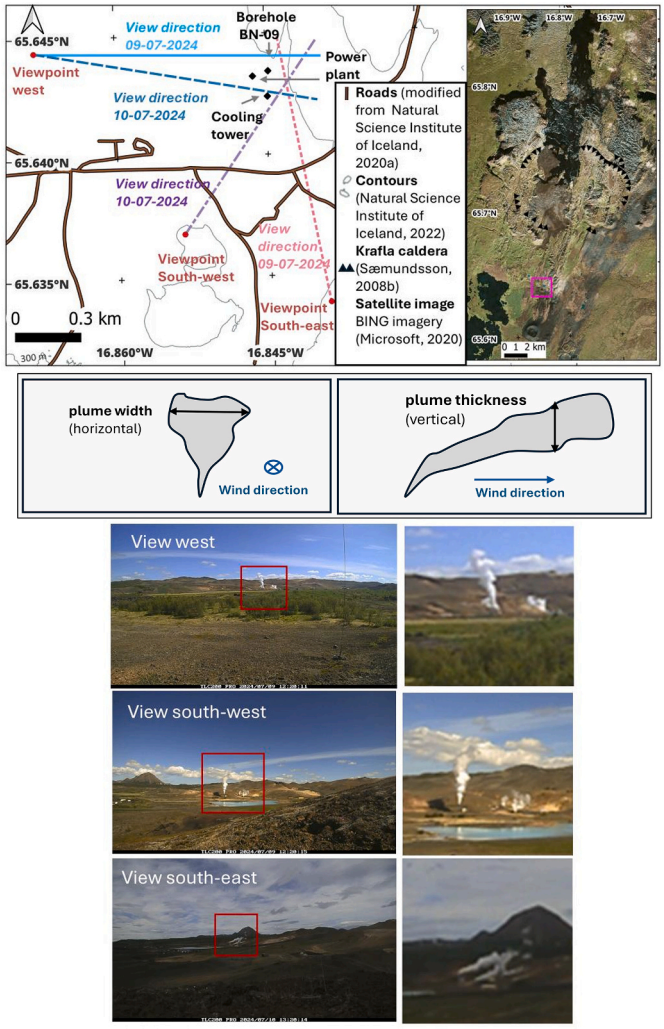

Fig. 5. Locations of the time-lapse photography of the steam plumes from the Bjarnarflag power plant (Natural Science Institute of Iceland, 2020a; Natural Science Institute of Iceland, 2022; Microsoft, 2022; Sæmundsson, 2008a).

diffuses quicker resulting in smaller steam clouds compared to periods of higher humidity. Linear regression of the data suggests likewise that the steam cloud area increases with humidity. The areas are assumed to have an error of about 15 %, as opaque and semi-opaque areas are detected visually. The shaded area in Fig. 6 shows mean humidity ±its standard derivation for the instances when aerial photographs were taken during the Krafla fires. The humidity values for the Bjarnarflag time-lapse photos in July 2024 are similar to those recorded at the time of the aerial photo acquisitions during the Krafla fires. Although there are indications for a positive correlation between humidity and plume size, the uncertainty is so high that the trend is not significant. As a result, we decided not to apply any correction to the aerial photographs from the Krafla fires. The relative humidity during the Krafla fires (h_{int}) was estimated using temporal and spatial interpolation (Eq. (6)), weighting humidity values (h_i) from different weather stations (Fig. 7) located 15–50 km from the eruption sites, by their inverse distance $(1/d_i)$ from the eruption site:

$$h_{int} = \left(\sum_{i=1}^{n}(1/d_i)h_i\right) \Big/ \left(\sum_{i=1}^{n}(1/d_i)\right) \quad (6)$$

The 4 stations did not measure humidity continuously. At each point in time, where the aerial photographs were taken, all available stations are used to interpolate the humidity data.

3.2.1.2. Scaling factor for Iceland. The observed correlation between the plume area and the thermal power of the power station, cooling tower and borehole BN09 at Bjarnarflag is shown in Fig. 8. The scatter is considerable while the values fit the adapted empirical relation of Hochstein and Bromley (2001). This indicates that the scaling factor derived from Hochstein and Bromley (2001) applies to Krafla/ Iceland. The maximum discrepancy between the true value and the mean value is 40 %. This reflects the considerable uncertainty in our estimates. Steam cloud area variations smaller than a factor of two should be regarded as scatter in the data. However, the method should be reliable for large changes in heat output, where steam cloud sizes changes are significantly larger than a factor of two.

3.2.2. Aerial photography analysis of the Krafla fires

The first eruption took place on the 20th of December 1975, with the following eight eruptions taking place between 1977 and 1984. The duration of the eruptions varied between 1 and 14 days (Einarsson et al., 1991). The timing of the aerial photographs of the Krafla fires, obtained from the archives of the National Land Survey of Iceland, varies from being taken during an ongoing eruption, and up to almost a year after the eruption. Opaque and semi-opaque areas of the observed steam clouds were visually determined and have therefore an uncertainty of around 15 %. Additionally, the angle of the sun may have minor influence how opaque the steam clouds appear in the photographs and contribute to the uncertainty. The thermal power was determined using Eqs. (2) and (3). In Table 1, there is an overview of the aerial photographs: their date and time, the flight line, flight height, and the days between the acquisition and the start/occurrence of the eruption preceding the time when the aerial photographs were taken. The timeline of intrusive events, eruptions and aerial photography for the whole period (1975–1985) is shown in Fig. 9. The different sets of aerial photographs are taken at very different times relative to the events, and only one acquisition was made between events. Our approach is to find the heat loss per meter of the volcanic fissure at the time of acquisition and then plot as a function of the time elapsed since the last eruption.

The aerial photographs were scanned at the National Land Survey of Iceland, using a photogrammetric scanner, Wehrli RM-6, with a scanning resolution of 20 μm. The Ground Resolved Distance of the aerial photographs ranges between 0.4 m (lowest flight height) to 0.7 m (highest flight height). Some of the images were mosaicked into a single orthomosaic using the Agisoft Metashape v2.0 software, having extracted manually picked ground control points from a recent, country-wide orthomosaic and Digital Elevation Model of Iceland (dem.lmi.is, National Land Survey of Iceland). Other images were visually georeferenced by using current satellite imagery. For visual interpretations, both, the raw scanned images as well as the orthomosaic, were used in this study.

4. Results

4.1. Energy input of the dyke

The geometrical parameters of the composite dyke formed incrementally during the Krafla fires were determined as follows:

- Length: The total horizontal extension of the dyke is up to 70 km to the North (e.g. Einarsson and Brandsdottir, 2021). Based on seismicity the dyke seems to intersect the full width of the high resistivity core at Krafla from south to north. The length of the dyke contributing to energy input in the geothermal system is therefore taken as being equivalent to 6.1–6.3 km.
- Width: The surface opening is constrained by the data of Tryggvason (1984) and Hollingsworth et al. (2012). The mean surface opening in the geothermal system is about 7.1 m using the optical image correlation and 7.8 m using geodetic measurements. Hollingsworth et al. (2013) estimated a ratio of dyke opening at depth to surface

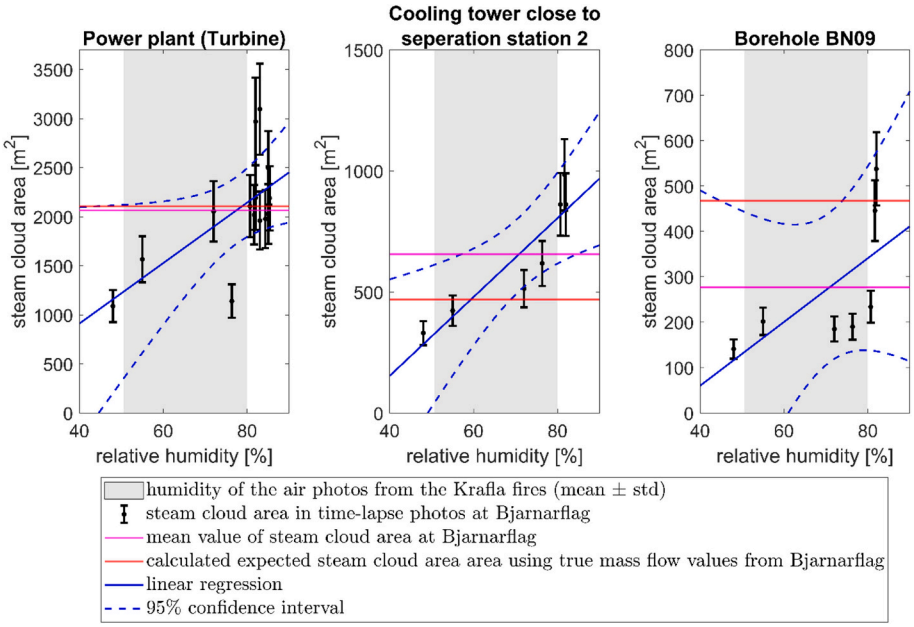

Fig. 6. Mass flow estimated by analyzing steam cloud areas of timelapse photography of the Bjarnarflag powerplant, NE-Iceland, from timelapse photography. The camera perspective is horizontal.

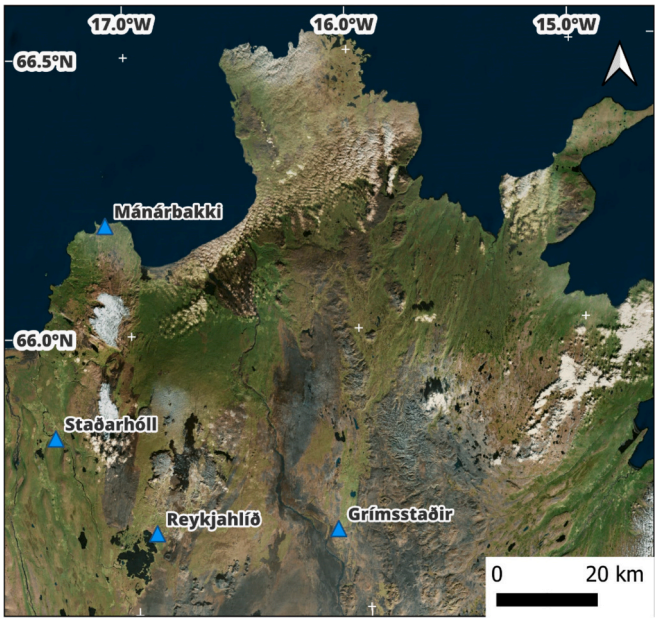

Fig. 7. Locations of weather stations. For the timelapse photography at the Bjarnarflag station the humidity of the Reykjahlið station was used. The humidity when the air photos were taken 1975–84 was calculated by using the distance-weighted average humidity of all the available stations. For e.g. the Reykjahlið station, there is not always humidity available during that time period (satellite image from Microsoft, 2022).

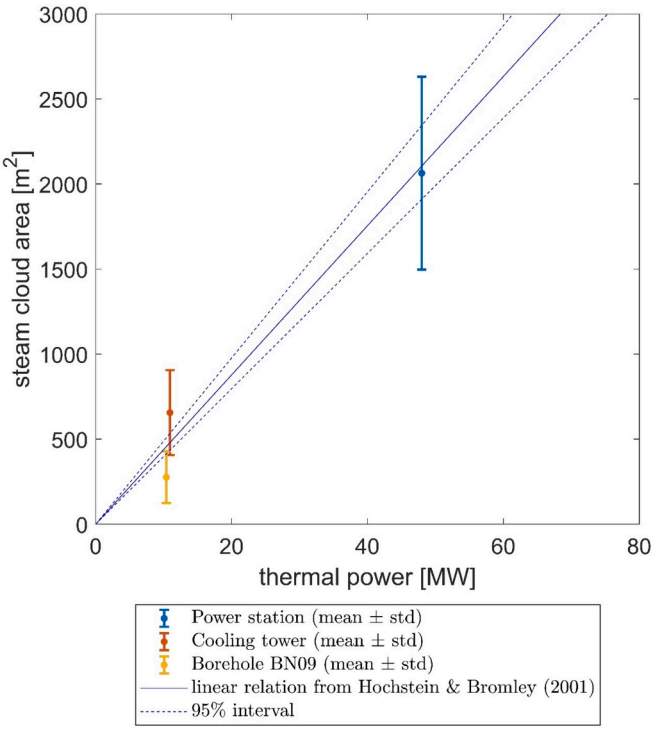

Fig. 8. Steam cloud area – thermal power at Bjarnarflag in July 2024, compared with the relationship of Hochstein and Bromley (2001). The thermal power is calculated from the known mass flow of steam.

extension as 1.25. Minimum and maximum estimates of the dyke width are therefore 8.9 m and 9.8 m.

- Height: Buck et al. (2006) estimated the total dyke height to be equal the thickness of the lithosphere, being 10 km at the plate boundary. Hollingsworth et al. (2013) assumed the dyke height to be between 2 km to 7 km. The dyke reaches the surface during eruptions while its top may be approximately at a depth of 600 m below the surface during the intrusive injections (Hollingsworth et al., 2013). As we are interested in the thermal effect of the dyke on the geothermal system, the depth extent of the permeable area has to be taken into account. During the Krafla fires earthquakes were mostly located in the uppermost 3 km while there was an aseismic zone, between 3 km to 7 km, that might be caused by a magma-rich zone/magma chamber (Einarsson, 1978; Einarsson and Brandsdottir, 2021). Other studies of seismic imaging found a strong attenuation at 2.7 km depth (Ágústsson et al., 2012), this is used as a minimum estimate for the dyke height. Experimental studies using temperature gradients of

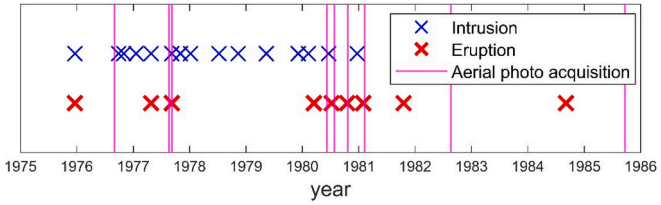

Fig. 9. Timeline of eruptions, intrusions, and acquisition of aerial photographs used in this study.

volcanic zones in Iceland indicated that geothermal fluids might circulate down to a depth of 4 km to 6 km (Violay et al., 2012). The average value of 5 km is therefore chosen as the maximum estimate of the depth at which the dyke can thermally affect the geothermal system.

Using the constraints above, the likely minimum and maximum estimates of the dyke volume and its thermal energy are presented in Table 2.

4.2. Energy loss by steaming

4.2.1. Location of steaming

The locations where transient steaming is seen in relation to the nine eruptions that occurred (lasting 1–14 days) on the aerial photographs are presented in Figs. 10–14. The characteristics of the steaming observed can be summarized as follows:

- Steaming was mainly present on and in the vicinity of the eruptive fissures. It was predominantly observed in the newly opened fissures of the ongoing or the most recent eruption prior to the time that the aerial photographs were taken. There was also steaming associated with previous eruptive fissures. This was especially prevalent for the fissure associated with the first eruption, where steaming occurred during or following later eruptions.
- The geothermal area of Leirhnjúkur was repeatedly reactivated after some eruptive events, with an increase in steaming.
- In some cases, lava flowed into faults or non-eruptive fissures and this downflow of lava often induced steaming at these faults/fissures. This is visible in the aerial photographs taken several days after the eruption of July 1980, October 1980, and January/ February 1981. Reports describe the forcing of lava into faults in July 1980 and February 1981, as well as the flow of lava into older fissures in November 1984 (Global Volcanism Program, 1980; Global Volcanism Program, 1981; Global Volcanism Program, 1984). For the eruption in September 1984, the aerial photographs available were taken 352 days after the eruption started. Such transient steaming due to lava flow into fissures is expected to have finished after such a long time.
- In the aerial photographs related to the first event, which were taken 257 days after the eruption, steaming is visible in a preexisting fissure close to the eruptive fissure.
- For the eruptive event of October 1980, the steam plume from the volcanic vent is visible in the aerial photographs. These aerial photographs were taken while the eruption was still ongoing (last day).

Table 2
Dimensions of the part of the composite dyke formed in 1975–1984 within the geothermal reservoir.

Parameter	Estimate		Data sources
	low	high	
Geometrical parameters of the dyke			
Length	6.1 km	6.3 km	Based on extent of geothermal system (Einarsson and Brandsdottir, 2021; Mortensen et al., 2015; Árnason and Magnússon, 2001)
Width	8.9 m	9.8 m	derived from Tryggvason (1984), Arnadottir et al. (1998), Hollingsworth et al. (2012) and Hollingsworth et al. (2013)
Height	2.7 km	5 km	derived from Ágústsson et al. (2012) and Violay et al. (2012)
Volume V	0.15 km^3	0.31 km^3	
Physical parameters of the dyke			
heat capacity c_p	1100 J/(kg °C)		Hartlieb et al. (2016)
density of the magma ρ	2750 kg/m^3		Sigmundsson et al. (1997)
latent heat L	3.95×10^5 J/kg		Lesher and Spera (2015), table 5.1
emplacement temperature T_m	1150 °C		Rooyakkers et al. (2024)
Average temperature of the geothermal system T_{sys}	300 °C (0 km to 2.7 km)	400 °C (0 km to 5 km depth)	based on borehole data of Mortensen et al. (2015)
Thermal energy of the dyke affecting the geothermal system	5.4×10^{17} J	1.0×10^{18} J	

4.2.2. Power of steaming

As previously discussed, most of the steam is rising from the eruptive fissures or very close to them. Moreover, the length of volcanic fissures varied between eruptions. In order to estimate the rate of steaming as a function of time since dyke intrusion, the calculated power of steaming from the plumes observed is normalized by the length of the volcanic fissures for each event. The results, demonstrated in Fig. 15, show that the steaming observed can be divided into two parts. Firstly, the high steaming, occurring during and immediately after the eruption, appears to decay approximately exponentially. Following this rapid decrease, the steaming reaches a semi-constant level. This change of the power of steaming with time, normalized by the fissure length, can be approximated with the following equation, a sum of the two terms:

$$P(t) = P'_{bg} + (P_0 - P'_{bg}) \cdot \exp(-d \cdot t) \quad (7)$$

Here P'_{bg} and P_0 are respectively the background power and initial power of steaming per unit length of fissure, t is the time since the onset of last eruption and d is a constant describing the decay of the rapidly declining part. The best fit values are $P'_{bg} = 5.3 \bullet 10^4\ W/m$, $P_0 = 8.1 \bullet 10^5\ W/m$ and $d = 8.44 \bullet 10^{-7}\ s^{-1}$.

4.2.3. Energy released by steaming

Since our aim is to assess the energy lost to the atmosphere by steaming from the geothermal system, due to heat lost from the feeder dyke, we use data obtained for the fissures within the geothermal system (see Table 3), and exclude plumes outside it, when integrating the power of steaming shown in Fig. 15. The energy released by constant/background steaming is calculated as:

$$E_{bg} = P'_{bg} \cdot \Delta t \cdot \overleftarrow{l}_{gts} \quad (8)$$

where P'_{bg} is the background steaming power as defined earlier Δt the duration of eruptive episode (9 years) and $\overleftarrow{l}_{gts}$ the average eruptive fissure length in the geothermal system. The exponential declining power within the geothermal system, where the fissure length for each event (i is eruptive event number, ranging from 1 to 9) is $l_{i.gts}$, is obtained from

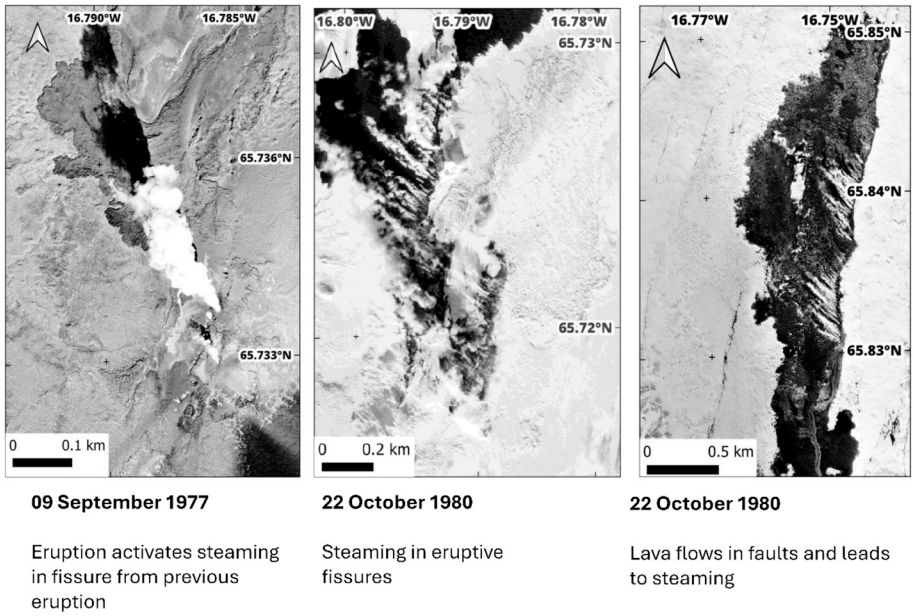

Fig. 10. Selected cutouts of the air photos showing different locations of steaming. Aerial photographs are acquired by Landmælingar Íslands (LMI, the National Land Survey of Iceland).

$$E_e = \int_0^{t'} \left(P_0 - P'_{bg}\right)\cdot\exp(-d\cdot t)dt\cdot\sum_{i=1}^{n} l_{i.gts} \tag{9}$$

Table 4 does not include steaming that occurred during the intrusive, non-eruptive events that took place in the period 1976–1979 where, at least in some cases, an increase in steaming was observed. Hence, the values in Table 4 may be an underestimate and the higher-end values of the best fit (~6–8 %) being the most probable for the fraction of the thermal energy lost to the atmosphere from the composite dyke. However, total uplift of the center of the Krafla caldera from 1976 to 1985 (from start to end the Krafla fires) was at least 3 m (e.g. Einarsson and Brandsdottir, 2021, Fig. 2) indicating that sills/intrusions other than the dyke may also have contributed heat to the geothermal system. The volume of these intrusions is uncertain, but an order of magnitude estimate can be made. If sills of 3 m thickness were intruded over an area equivalent to that of the present surface manifestation of the Krafla geothermal system (10 km^2), the volume would be similar to 0.03 km^3, close to 10–20 % of the volume of the dyke (Table 2). This is not accounted for in our calculations and may to an extent offset the possible underestimate due to steaming during the intrusive events.

5. Discussion

5.1. Interpretation

The exponential decay of steaming, seen in Fig. 15, is interpreted as the interaction of the dyke with the shallow groundwater/geothermal water (Fig. 16). Effects from the feeder dyke at greater depth as well as deeper intrusions are less likely to lead to an immediate increase in steaming. This is because the heat released from the magma would mostly be dissipated by heating of the geothermal water without major boiling occurring in most cases. It is only when the geothermal reservoir is at or near boiling point conditions near to the surface, that dyke formation is expected to lead to major steaming. In many cases where the reservoir temperature is significantly below the boiling point, local steam formation at a depth near the dyke would not rise to the surface. Instead, it creates a more diffused thermal signal, the constant/ background steaming. The surface lava formed in each event is considered to have negligible thermal effects on the geothermal system. The lava is all emplaced on the surface, well above the groundwater table, and hence downward heating would be mostly by conduction. The conductivity of lava is quite low, and the bottom of the lava usually has some scoria which effectively acts as an insulator. This was for example observed where lava advanced on the top of firn during the 2010 effusive Fimmvörðuháls eruption (Edwards et al., 2012), preceding the summit eruption at Eyjafjallajökull.

Assuming that the energy lost to the atmosphere by steaming is 4–8 % of the total thermal energy of the dyke, this corresponds to the energy found in the top 110–400 m of a 2.7–5 km high dyke. At greater depths, the interaction of the dyke with the geothermal water in the permeable rocks might result in much faster heat loss from the dyke than found by conduction only (e.g. Reynolds et al., 2017). However, where the temperature of the geothermal water is considerably below the boiling point, heat extraction by the geothermal water will enhance the cooling of the dyke and heating the water without extensive boiling. If boiling happens at greater depth, the advection of the steam might take up to several months, depending on the permeability of the geothermal system. The rising velocity can be estimated from

$$v = \left(v_{Darcy}/\Phi\right) = -k/(\mu\phi)\cdot((dp/dz) - \rho g) \tag{10}$$

with v_{Darcy} being the Darcy velocity, Φ the porosity, (dp/dz) the pressure gradient in z-direction (downwards), ρ, μ respectively the density and viscosity of the steam, and k the permeability of the geothermal system (Faust and Mercer, 1979; Hayba and Ingebritsen, 1997; Huyakorn and Pinder, 1983). Assuming an intrusion at 500 m depth in a fully saturated medium near the boiling point with a porosity of 10 %, at a pressure of 40 bar and a steam temperature slightly above the boiling point at 251 °C, the rising times, assuming a constant velocity, would be around 13 days for permeability of 1×10^{-13} m^2 and 130 days for permeability of 1×10^{-14} m^2. The deeper the steam is located, the lower its rising velocity, as its density and viscosity increase. Moreover, any steam generated at this depth may condense as it rises through a considerable thickness of groundwater-saturated rock at sub-boiling temperatures.

5.2. Possible effects of thermal fracturing, precipitation and condensation

5.2.1. Role of thermal fracturing

As Fig. 15 indicates, most of the heat released into the atmosphere with steaming occurs in the first 50–100 days. This time scale can be

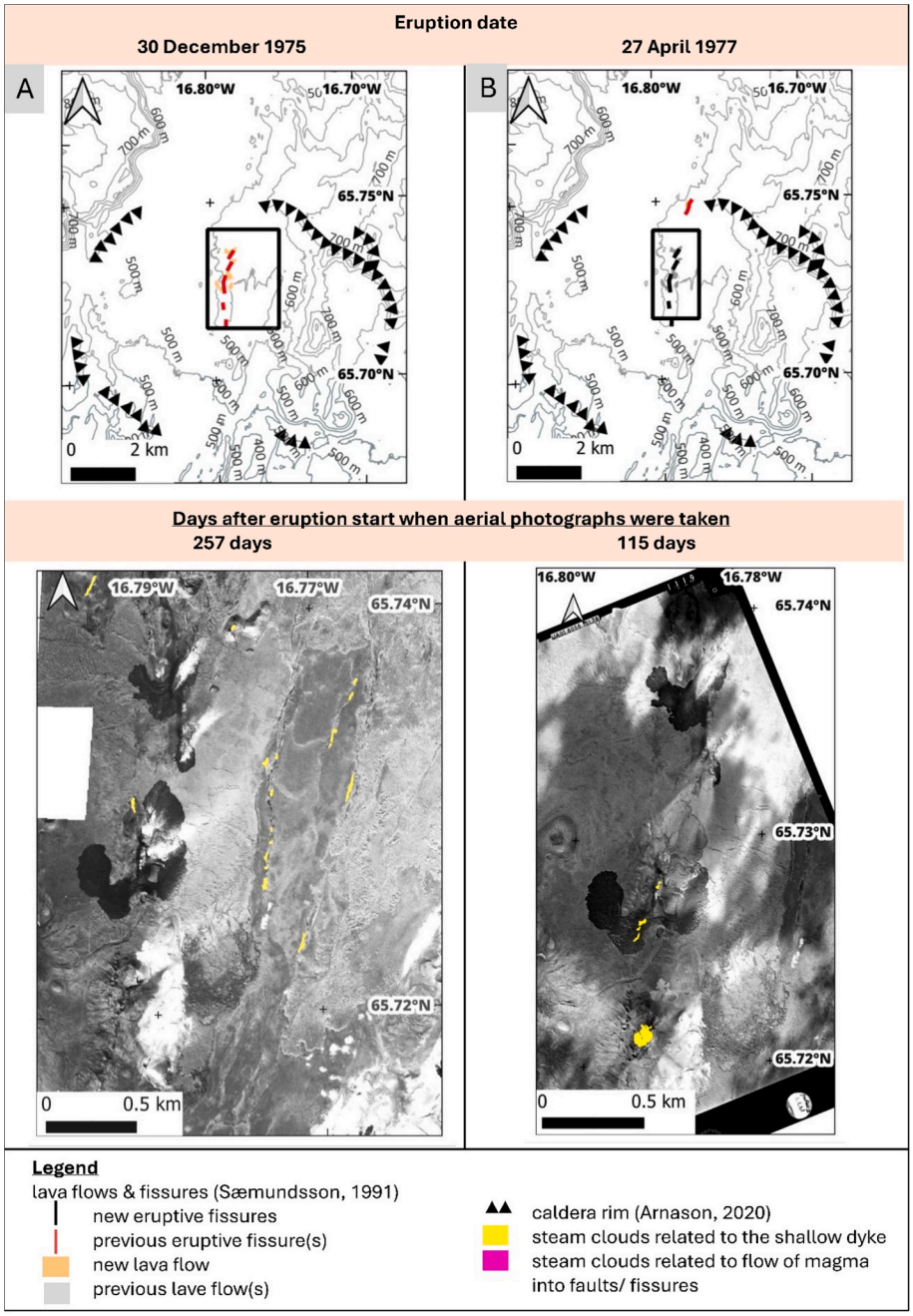

Fig. 11. Steaming related to the feeder dyke heat loss (marked in yellow), visible in the air photos taken during or after each eruptive event during the Krafla fires. Aerial photographs are acquired by Landmælingar Íslands (LMI, the National Land Survey of Iceland). (For interpretation of the references to colour in this figure legend, the reader is referred to the web version of this article.)

compared to the solidification time of a dyke, using analytical solutions by Turcotte and Schubert (2014). It is assumed that there is one initial temperature of the dyke and that the same applies to the geothermal system. Endmember cases for the surrounding rock are (a) no permeability and heat loss by conduction only and (b) infinite vigor of convection resulting in the temperatures of the surrounding rock remaining constant. The solidification time t_s can be estimated the following:

$$t_s = (w/4\eta_s)^2(1/\kappa) \tag{11}$$

with w being the width of the dyke, κ the thermal diffusivity, k the thermal conductivity and ρ the density of the solidified rock. η_s can be determined with this relationship below assuming an only conductive host rock

$$L\sqrt{\pi}/(c(T_m - T_0)) = exp(-\eta_s^2)/((1 + erf(\eta_s))\eta_s) \tag{12}$$

or host rock at a constant temperature

$$L\sqrt{\pi}/(c(T_m - T_0)) = exp(-\eta_s^2)/(erf(\eta_s)\eta_s) \tag{13}$$

with L being the latent heat, c the heat capacity, T_m the magma temperature, T_0 the initial temperatures of the host rock/geothermal system and erf $erf(\,)$ the error function. By setting the ambient temperature T_0 to 100 °C and κ to 6×10^{-7} m/s^2 (Hartlieb et al., 2016) with all other values taken from Table 2, a 1 m dyke would solidify next to the conductive host rock in 2.8 days and in 1.5 days for host rock at a constant temperature. For a 2 m thick dyke these values are 5.9 and 11.3

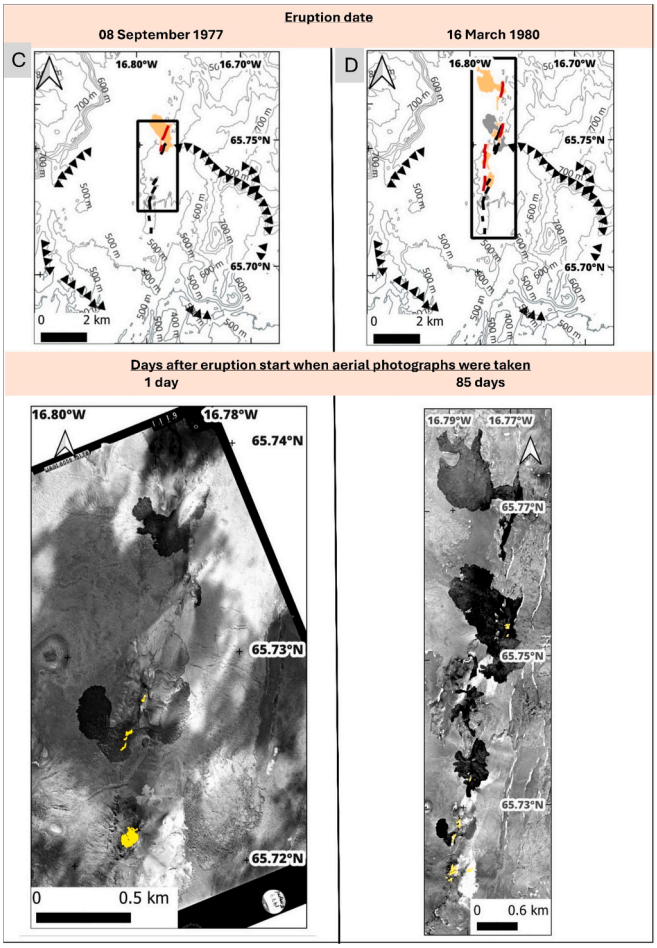

Fig. 12. Steaming related to the feeder dyke heat loss (marked in yellow), visible in the air photos taken during or after each eruptive event during the Krafla fires. Legend in Fig. 10. Aerial photographs are acquired by Landmælingar Íslands (LMI, the National Land Survey of Iceland). (For interpretation of the references to colour in this figure legend, the reader is referred to the web version of this article.)

days. These cooling times are a good estimation for the first dyke injection. Later dykes are considered to be injected into the previous, presumably solidified intrusion. Therefore, the surrounding temperature might be higher, and solidification times slightly longer. Comparing this to heat release estimated from the aerial photographs, see Fig. 15, about 1/3 of the total heat loss during the first 50–100 days, happens in the first five to six days. This is in reasonable agreement with what should be expected for the cooling rates presented above. As there is scatter in the data, it is difficult to estimate from these calculations only, which of the two end member cases is closer to being the dominant heat transfer mechanism. The water table in the caldera in vicinity at the 1975–1984 eruption sites is at 10–60 m depth. As the water table is very close to the surface, convection of the fluid cannot be neglected. As the steam rises directly from the eruptive fissures, it can be assumed that the solidified dyke and its immediate surroundings is a permeable pathway, and that thermal fracturing plays a role. These small fractures are pathways for water and would lead to faster heat mining. For the volcanic/geothermal systems on the Reykjanes Peninsula, studies show that dykes create vertical permeability (Sæmundsson et al., 2020).

5.2.2. Role of precipitation

Evaporation of precipitation seeping downwards along the fractures formed in the surface is a potential contribution to cooling of the dyke. This energy can be estimated as

$$E_{prec} = j_m \cdot \left(c_{p,H2O} \cdot \Delta T + L_{H2O,vap}\right) \cdot \Delta t \cdot \bar{l}_{gts} \cdot w_{surf} \quad (14)$$

Here j_m is the yearly mass of precipitation per unit area (30-year annual average for 1961–1990 in Reykjahlið is 435 mm) (Icelandic Meteorological Office, 2012) equivalent to 435 kg/ m^2. $L_{H2O,vap}$ is the latent heat of water of vaporization, $c_{p,H2O}$ is the heat capacity of water, ΔT the temperature difference between emplacement and the boiling temperature (≈ 100 °C), Δt is the duration of the eruptive episode (9 years), $\bar{l}_{gts}$ is the average length of a fissure in a geothermal system, and w_{surf} is the surface opening of the fissure. The value obtained is $2.4 - 2.7 \times 10^{14}$ J, suggesting that less than 1 % of the steaming may be caused by evaporation of precipitation entering the fissure, so this can be neglected.

5.2.3. Role of condensation

When the steam rises in porous rock, it may partly or fully condense before reaching the surface. Looking at the geothermal field at the Krafla mountain and Leirhnjúkur today, Bini et al. (2024) estimated a heat release by condensation of 144 ± 40 MW. Over nine years the heat released by condensation would be $4.1 \pm 0.1 \times 10^{16}$ J, similar to the background steaming in the fissures. In our setting, we look at steaming caused by fissure eruptions, where condensation might be less important. Firstly, the steam rises into a system very close to the boiling point, so intensive heat loss of the rising fluid is not expected. Secondly, in places the surface is overlain by the newly erupted lava flow. In both settings, near surface condensation could only happen in the uppermost part of the surface where the magma is already solidified and cooled down to below 100 °C; a process that should take considerably longer than the months required for the solidification of a few meters' thick lava flow (e.g. Turcotte and Schubert, 2014, Figs. 4–33).

5.2.4. Effect of exploitation

The exploitation of Krafla started in 1977 but at a very low production rate during the Krafla fires (e.g. Mortensen et al., 2015). The exploited drillholes were located 1–2 km to the east of the active volcanic fissures and the effect on steaming related to the dyke formation and cooling during the observation period (1975–1985) is considered to have been negligible.

5.3. Comparison with other studies

In his numerical heat transfer model of Krafla, Bodvarsson et al. (1984) determined Hveragil as the main upflow zone of high-enthalpy fluid with a heat release of approximately 0.0225 MW/m which is very similar to the low end-member estimation of the background steaming, see Fig. 15.

The geothermal area in Reykjanes has a heat loss by steaming determined by anemometer measurements of 71 ± 14 MW (Fridriksson et al., 2006). The maximum steaming determined in this study was around 0.86 MW/m, directly after the eruption started. Considering the average length of the eruptive fissures in the geothermal system in Krafla, the power of maximum steaming would be similar to 2200 MW, around 2 orders of magnitude higher than e.g. seen at the Reykjanes area.

Cherkaoui et al. (1997) studied the heat flow of hydrothermal plumes on the seafloor at the coaxial segment of the Juan de la Fuca ridge. The hydrothermal plume detected above the seafloor is assumed to have been caused by a dyke injection. A graph showing heat flux per meter along the source over time shows a similar exponential decay as observed in our study. The curve starts at around 10 MW/m and decays in 100 days to 1 MW/m and fits the cooling of 500 m deep, 4 m wide intrusion in a host rock with very high permeability, 10×10^{-11} m^2. The power of heat loss was about one order of magnitude higher than observed at Krafla. In addition to the high permeability, a contributing

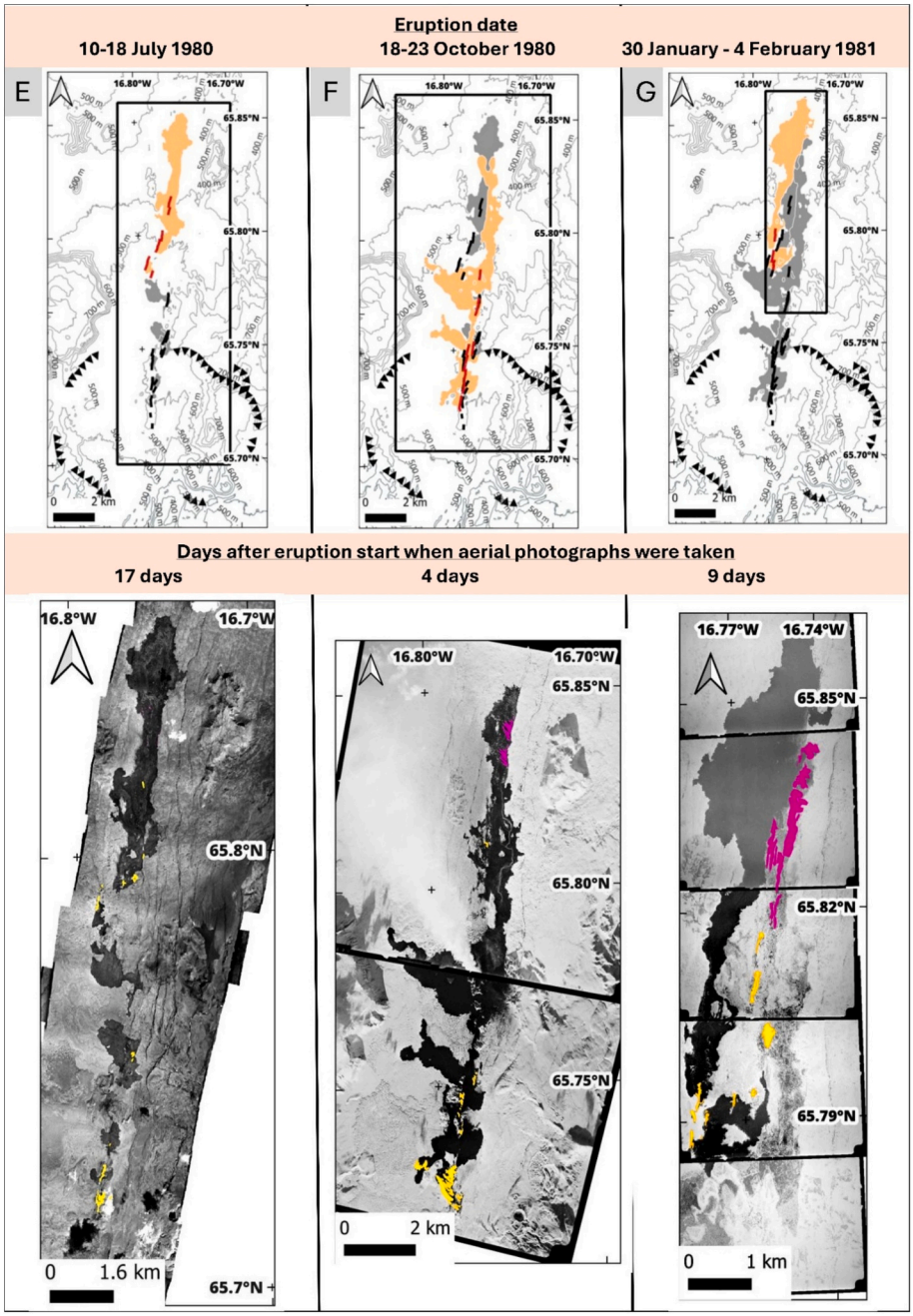

Fig. 13. Steaming related to the feeder dyke heat loss (marked in yellow), visible in the air photos taken during or after each eruptive event during the Krafla fires. Steaming related due to lava flow in faults and previous fissures, marked in pink. Legend can be found in Fig. 10. Aerial photographs are acquired by Landmælingar Íslands (LMI, the National Land Survey of Iceland). (For interpretation of the references to colour in this figure legend, the reader is referred to the web version of this article.)

factor may have been the greater width of the dyke, 4 m, compared to 0.5–1 m per event at the Krafla fires. Another reason could be that the heat loss dynamics are different. In a setting of atmosphere and rock, the water has to be heated up to boiling temperatures to rise to the atmosphere. The water in a permeable system below the seafloor will convect vigorously and does not require boiling to do so.

6. Conclusions

We applied the method of Hochstein and Bromley (2001) to determine the heat output by steaming associated with fissure eruptions from the size of steam plumes observed on vertical aerial photographs obtained during the Krafla fires. The energy of the dyke brought into the geothermal systems was based on volume estimates derived from seismic, geodetics, and optical image correlation. The main results of this study are:

- The part of the large composite dyke formed within the geothermal reservoir of Krafla during the Krafla fires (~9–10 m wide, ~6 km long and with a height in the range 2.7–5.0 km) is considered to have had a volume of 0.15–0.31 km^3.
- The thermal energy released from the composite dyke within the geothermal reservoir is estimated as 0.5–1.0 × 10^{18} J. Thereof, the thermal energy loss to the atmosphere by steaming is estimated similar to 5–10 %. This indicates that 90–95 % of the thermal energy

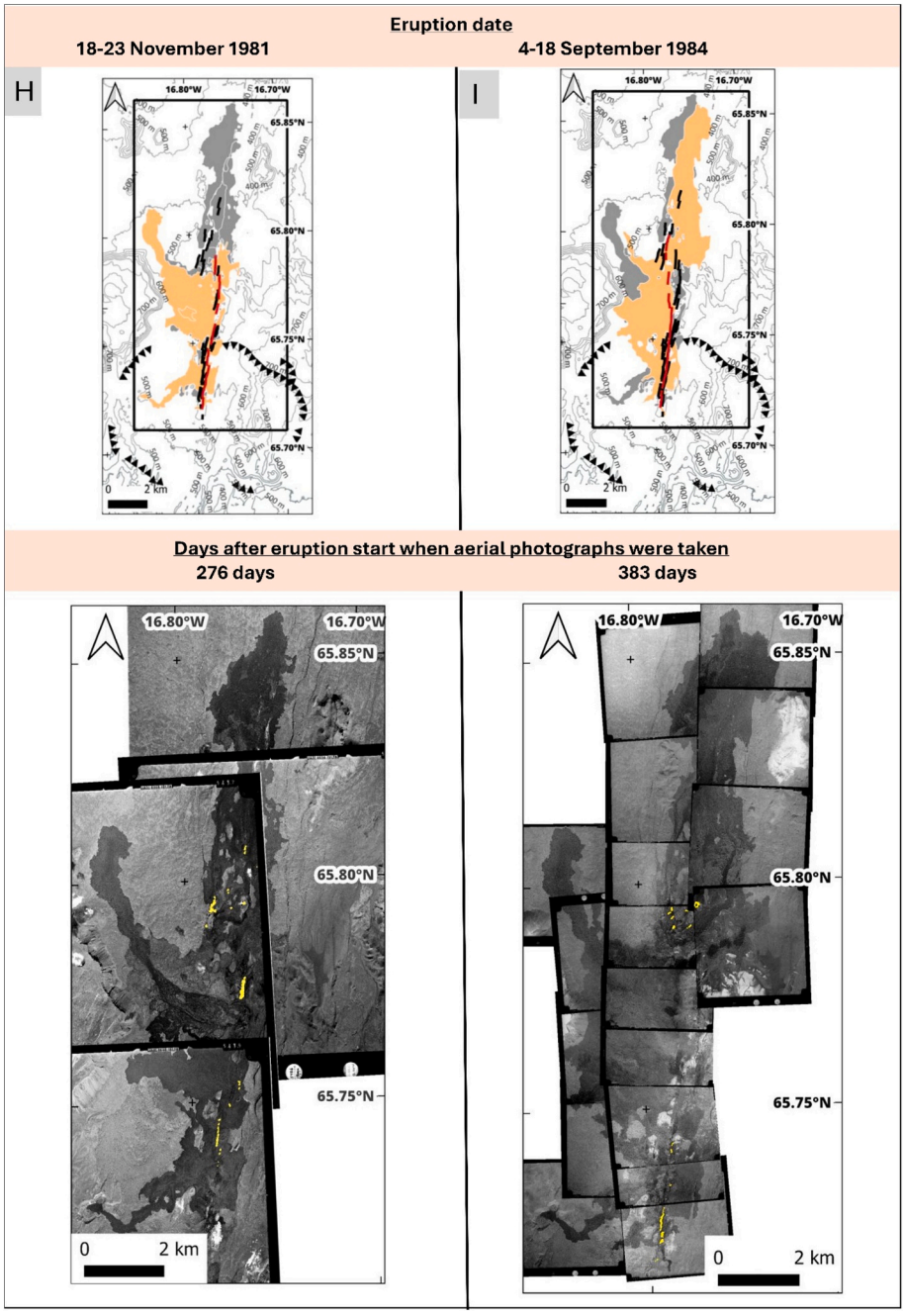

Fig. 14. Steaming related to the feeder dyke heat loss (marked in yellow), visible in the air photos taken during or after each eruptive event during the Krafla fires. Legend can be found in Fig. 10. Aerial photographs are acquired by Landmælingar Íslands (LMI, the National Land Survey of Iceland). (For interpretation of the references to colour in this figure legend, the reader is referred to the web version of this article.)

remains within the geothermal reservoir and is released over much longer timescales.

- Steaming decays exponentially over 1.5–3 months after the eruption, from an initial thermal power per fissure length of ~0.9 MW/m to a background level of 0.05 MW/m. This behavior suggests that steaming is mostly driven by the interaction of the feeder dyke with the shallow groundwater/geothermal water, as the steaming is mostly rising along the eruptive fissures.
- Most of the heat brought into the upper crust by the intruded magma appears to be released and dissipated into the geothermal reservoir over longer time scales than observed for the shallow, short-term steaming.

CRediT authorship contribution statement

Patricia Fehrentz: Writing – original draft, Visualization, Software, Methodology, Investigation, Formal analysis, Data curation. **Magnús T. Gudmundsson:** Writing – review & editing, Supervision, Project administration, Methodology, Investigation, Funding acquisition, Data curation, Conceptualization. **Hannah I. Reynolds:** Writing – review & editing, Supervision, Methodology. **Anette K. Mortensen:** Writing – review & editing, Resources, Data curation. **Sydney R. Gunnarson:** Writing – review & editing, Resources, Data curation. **Joaquin M.C. Belart:** Writing – review & editing, Resources, Data curation. **Michaela A. Chodora:** Writing – review & editing, Visualization, Investigation.

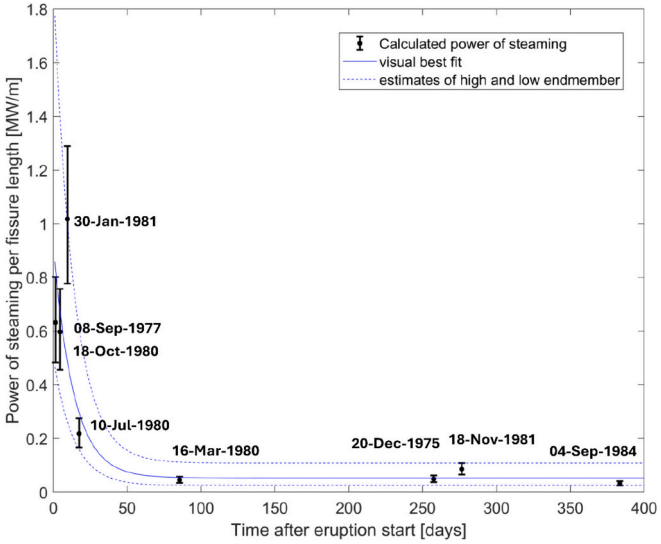

Fig. 15. Temporal heat output by steaming after eruption start of the Krafla fires. Heat output is normalized by fissure length. Dates close to the data points mark the onset of eruption. The eruption of 27 April 1977 is excluded, as air photos only show the previous and not the current eruption area.

Table 3
Eruptive fissure length for each event. Total fissure length was summarized by Harris et al. (2000) (based on Björnsson, 1985; Björnsson et al., 1979; Björnsson et al., 1977; Grönvold, 1982; Grönvold, 1983; Grönvold, 1987; SEAN, 1989). Fissure length in the geothermal system was determined using maps by Sæmundsson (1991).

Eruptive event no.	Total fissure length [m]	Fissure length within geothermal system [m]
1	2000	2000
2	3000	1800
3	900	0
4	4500	900
5	4000	0
6	7000	2000
7	2000	0
8	8500	2300
9	8500	2400
	Total number of eruptive events	**Number of eruptive events in the geothermal system**
1–9	9	6
	Average fissure length [m]	**Average fissure length in the geothermal system [m]**
1–9	4190	1900

Table 4
Absolute heat output by steaming and percental heat loss of the dyke's energy.

	Best fit	Low end member	High end member
	Heat output of steaming [J]		
Background steaming E_{bg}	2.9×10^{16}	1.3×10^{16}	5.9×10^{16}
Steaming after feeder dyke injection E_e	1.2×10^{16}	6.4×10^{15}	2.4×10^{16}
Total steaming $E_{tot} = E_{bg} + E_e$	4.0×10^{16}	2.0×10^{16}	8.3×10^{16}
	Energy loss of the dyke by steaming [%]		
Heat output by steaming to thermal energy of the dyke	4–8 %	2–4 %	8–15 %

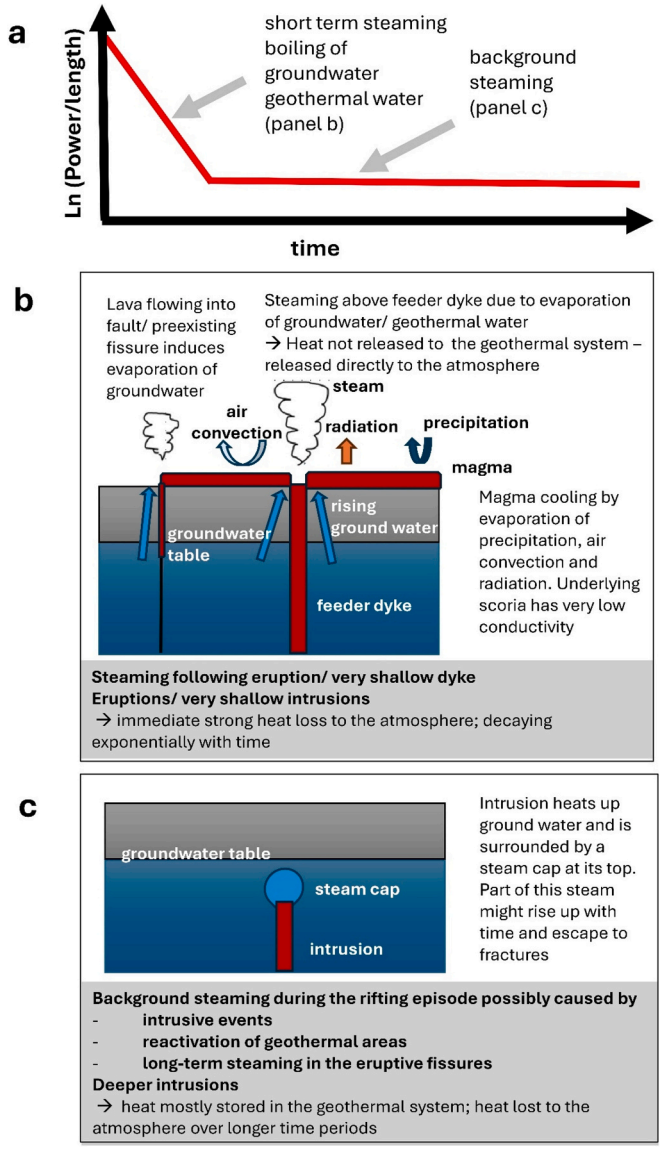

Fig. 16. Schematic summary of heat loss during eruptive and intrusive events in the Krafla fires (see Fig. 15).

Declaration of competing interest

The authors declare that they have no known competing financial interests or personal relationships that could have appeared to influence the work reported in this paper.

Acknowledgments

This work is funded by the European Union's Horizon 2020 research and innovation programme under the Marie Skłodowska-Curie grant agreement No 858092 - IMPROVE (www.improve-etn.eu). We would like to thank the Icelandic mapping service for providing the aerial photographs and acknowledge the support from Landsvirkjun, allowing fieldwork in their geothermal areas. Halldór Björnsson at IMO supplied weather data from the time of the Krafla fires. Thanks to Sveinbjörn Steinþórsson and Daniel G. Villarroel for conducting the fieldwork and first aid when needed. Thanks also to Jean Vandemeulebrouck, Yilin Yang, and Páll Einarsson for valuable discussions. The constructive and thoughtful comments by two anonymous reviewers improved the quality of this paper. Maps were plotted with QGIS, code was written, and graphs were plotted in MATLAB. GIMP and Microsoft PowerPoint

were used for the generation of figures. The BING satellite imagery was used.

Data availability

Data can be accessed under the following link: https://osf.io/sjd4g/?view_only=92a7b9fe342944b7a90ca5617bc4d1cb

References

Ágústsson, K., Flóvenz, Ó.G., Guðmundsson, Á., Árnadóttir, S., 2012. Induced seismicity in the Krafla high temperature field. GRC Transactions 36 (2012), 975–980.

Arnadottir, T., Sigmundsson, F., Delaney, P., 1998. Sources of crustal deformation associated with the Krafla, Iceland, eruption of September 1984. Geophys. Res. Lett. 25 (7). https://doi.org/10.1029/98GL50655.

Arnason, K., 2020. New conceptual model for the magma-hydrothermal-tectonic system of Krafla, NE Iceland. Geosciences 10 (1). https://doi.org/10.3390/geosciences10010034.

Árnason, K., Magnússon, I.Þ., 2001. Niðurstöður viðnámsmælinga í Kröflu. Orkustofnun.

Arnason, K., Karlsdottir, R., Eysteinsson, H., Flóvenz, Ó., Gudlaugsson, S.T., 2000. The Resistivity Structure of High-Temperature Geothermal Systems in Iceland, Proceedings of the World Geothermal Congress 2000. Kyushu-Tohoku, Japan, pp. 923–928.

Benjamínsson, J., Hauksson, T., 1998. Kröflusvæði og Námafjall. Yfirborðsathuganir og efnagreiningar haustið 1997. In: Yfirlit um Kröflusvæðið. Landsvirkjun – Kröflustöð, p. 104.

Benjamínsson, J., Hauksson, T., 2001. Kröflusvæði og Bjarnarflag. In: Umhverfisvöktun 2001. Landsvirkjun – Kröflustöð, p. 41.

Benjamínsson, J., Hauksson, T., 2004. Kröflusvæði og Bjarnarflag. Umhverfisvöktun 2004, p. 27.

Benjamínsson, J.H., Trausti, 1990. Kröflusvæði. Rannsóknir á gufuaugum 1990, p. 43.

Benjamínsson, J.H., Trausti, 1995. Kröflusvæði og Námafjall. Yfirborðsathuganir haustin 1994 og 1995, p. 20.

Bini, G., Chiodini, G., Ricci, T., Sciarra, A., Caliro, S., Mortensen, A.K., Martini, M., Mitchell, A., Santi, A., Costa, A., 2024. Soil CO2 emission and stable isotopes (δ13C, δ18O) of CO2 and calcites reveal the fluid origin and thermal energy in the supercritical geothermal system of Krafla, Iceland. J. Volcanol. Geotherm. Res. 447, 108032.

Björnsson, A., 1985. Dynamics of crustal rifting in NE Iceland. J. Geophys. Res. Solid Earth 90 (B12), 10151–10162.

Bjornsson, H., Gudmundsson, M.T., 1993. Variations in the thermal output of the Subglacial Grimsvotn Caldera, Iceland. Geophys. Res. Lett. 20 (19), 2127–2130.

Björnsson, A., Saemundsson, K., Einarsson, P., Tryggvason, E., Grönvold, K., 1977. Current rifting episode in North Iceland. Nature 266 (5600), 318–323.

Björnsson, A., Johnsen, G., Sigurdsson, S., Thorbergsson, G., Tryggvason, E., 1979. Rifting of the plate boundary in North Iceland 1975–1978. J. Geophys. Res. Solid Earth 84 (B6), 3029–3038.

Bodvarsson, G., 1982. Terrestrial energy currents and transfer in Iceland. Cont. Ocean. Rifts 8, 271–282.

Bodvarsson, G., Pruess, K., Stefansson, V., Eliasson, E., 1984. The Krafla Geothermal-Field, Iceland. 2. The Natural State of the System. Water Resour. Res. 20 (11), 1531–1544.

Buck, W.R., Einarsson, P., Brandsdottir, B., 2006. Tectonic stress and magma chamber size as controls on dike propagation: Constraints from the 1975-1984 Krafla rifting episode. J. Geophys. Res. Solid Earth 111 (B12).

Cherkaoui, A.S., Wilcock, W.S., Baker, E.T., 1997. Thermal fluxes associated with the 1993 diking event on the CoAxial segment, Juan de Fuca Ridge: a model for the convective cooling of a dike. J. Geophys. Res. Solid Earth 102 (B11), 24887–24902.

Edwards, B., Magnússon, E., Thordarson, T., Guðmundsson, M.T., Höskuldsson, A., Oddsson, B., Haklar, J., 2012. Interactions between lava and snow/ice during the 2010 Fimmvörðuháls eruption, south-Central Iceland. J. Geophys. Res. Solid Earth 117 (B4).

Einarsson, P., 1978. S-wave shadows in the Krafla caldera in NE-Iceland, evidence for a magma chamber in the crust. Bull. Volcanol. 41, 187–195.

Einarsson, P., Brandsdottir, B., 2021. Seismicity of the Northern Volcanic Zone of Iceland. Front. Earth Sci. 9.

Einarsson, P., Gardarsson, A., Einarsson, A., 1991. The Krafla rifting episode 1975–1989. In: Náttúra Mývatns (The Nature of Lake Mývatn), pp. 97–139. ISBN 9979906502.

Faust, C.R., Mercer, J.W., 1979. Geothermal reservoir simulation: 1. Mathematical models for liquid-and vapor-dominated hydrothermal systems. Water Resour. Res. 15 (1), 23–30.

Fridriksson, T., Kristjansson, B., Armannsson, H., Margretardottir, E., Olafsdottir, S., Chiodini, G., 2006. CO2 emissions and heat flow through soil, fumaroles, and steam heated mud pools at the Reykjanes geothermal area, SW Iceland. Appl. Geochem. 21 (9), 1551–1569.

Gislason, G., Armannsson, H., Hauksson, T., 1978. Krafla: Hitaastand og gastegundir i jardhitakerfinu, Rep, OS/JHD-7846. Natl. Energy Auth, Reykjavik, Iceland.

Global Volcanism Program, 1980. Report on Krafla (Iceland). In: Squires, D. (Ed.), Scientific Event Alert Network Bulletin, 5(7). Smithsonian Institution. https://doi.org/10.5479/si.GVP.SEAN198007-373080.

Global Volcanism Program, 1981. Report on Krafla (Iceland). In: McClelland, L. (Ed.), Scientific Event Alert Network Bulletin, 6(2). Smithsonian Institution. https://doi.org/10.5479/si.GVP.SEAN198102-373080.

Global Volcanism Program, 1984. Report on Krafla (Iceland). In: McClelland, L. (Ed.), Scientific Event Alert Network Bulletin, 9(11). Smithsonian Institution. https://doi.org/10.5479/si.GVP.SEAN198411-373080.

Grönvold, K., 1982. Krafla. Bull. Volcanic Eruptions 20, 91–92.

Grönvold, K., 1983. Krafla. Bull. Volcanic Eruptions 21, 78–79.

Grönvold, K., 1987. Krafla. Bull. Volcanic Eruptions 24, 51–52.

Harris, A., Murray, J., Aries, S., Davies, M., Flynn, L., Wooster, M., Wright, R., Rothery, D., 2000. Effusion rate trends at Etna and Krafla and their implications for eruptive mechanisms. J. Volcanol. Geotherm. Res. 102 (3–4).

Hartlieb, P., Toifl, M., Kuchar, F., Meisels, R., Antretter, T., 2016. Thermo-physical properties of selected hard rocks and their relation to microwave-assisted comminution. Miner. Eng. 91, 34–41.

Hayba, D.O., Ingebritsen, S.E., 1997. Multiphase groundwater flow near cooling plutons. J. Geophys. Res. Solid Earth 102 (B6), 12235–12252.

Hjartardottir, A.R., Einarsson, P., Bramham, E., Wright, T.J., 2012. The Krafla fissure swarm, Iceland, and its formation by rifting events. Bull. Volcanol. 74 (9).

Hjartardóttir, Á., Einarsson, P., Magnúsdóttir, S., Björnsdóttir, Þ., Brandsdóttir, B., 2016. Fracture Systems of the Northern Volcanic Rift Zone. An onshore part of the Mid-Atlantic plate boundary, Iceland.

Hochstein, M., Bromley, C., 2001. Steam cloud characteristics and heat output of fumaroles. Geothermics 30 (5), 547–559.

Hollingsworth, J., Leprince, S., Ayoub, F., Avouac, J.-P., 2012. Deformation during the 1975-1984 Krafla rifting crisis, NE Iceland, measured from historical optical imagery. J. Geophys. Res. Solid Earth 117.

Hollingsworth, J., Leprince, S., Ayoub, F., Avouac, J.-P., 2013. New constraints on dike injection and fault slip during the 1975-1984 Krafla rift crisis, NE Iceland. J. Geophys. Res. Solid Earth 118 (7).

Huyakorn, P.S., Pinder, G.F., 1983. Computational Methods in Subsurface Flow. Academic Press.

Natural Science Institute of Iceland, 2020a. IS 50V Samgongur. https://www.lmi.is/is/landupplysingar/gagnagrunnar/is-50v/samgongur accessed 08-Feb-2025.

Natural Science Institute of Iceland, 2020b. IS 50V Strandlína. https://www.lmi.is/is/landupplysingar/gagnagrunnar/is-50v/strandlina accessed 08-Feb-2025.

Icelandic Meteorological Office, 2012. Climatological Data. description. https://en.vedur.is/climatology/data/. data. https://en.vedur.is/Medaltalstoflur-txt/Reykjahlid_468_med6190.txt. accessed.

Icelandic Meteorological Office, 2022. SurfaceWaterBody IS 20220322. https://hub.arcgis.com/datasets/vedur::surfacewaterbody-is-20220322/about accessed 08-Feb-2025.

Jarosch, A.H., Magnússon, E., Hannesdóttir, K., Belart, J.M., Pálsson, F., 2023. Geothermal heat source estimations through ice flow modelling at Mýrdalsjökull, Iceland. Cryosphere 18 (5), 2443–2454. https://doi.org/10.5194/tc-18-2443-2024.

Lesher, C.E., Spera, F.J., 2015. Thermodynamic and transport properties of silicate melts and magma. In: The Encyclopedia of Volcanoes. Elsevier, pp. 113–141.

Microsoft, 2022. BING Imagery. https://learn.microsoft.com/en-us/bingmaps/rest-services/imagery/get-imagery-metadata accessed 08-Feb-2025.

Mortensen, A.K., Guðmundsson, Á., Steingrímsson, B., Sigmundsson, F., Axelsson, G., Ármannsson, H., Björnsson, H., Ágústsson, K., Sæmundsson, K., Ólafsson, M., Karlsdóttir, S., Halldórsdóttir, R., Hauksson, T., 2015. The Krafla Geothermal System. Research Summary and Conceptual Model Revision. Landsvirkjun.

National Landsurvey of Iceland (Landmælingar), 1977–1985. Gallery of Aerial Photography (Loftmyndasafn). https://www.lmi.is/is/vefsjar/korta-og-loftmyndasofn/loftmyndasafn.

Natural Science Institute of Iceland, 2022. ÍslandsDEM útgáfa 1.0. accessed 08-Feb-2025 https://dem.gis.is/mapview/?application=DEM.

Oddsson, B., 2016. Heat transfer in volcanic settings: Application to lava-ice interaction and geothermal areas, PhD dissertation, Faculty of Earth Science, University of Iceland, 99 pp. https://skemman.is/bitstream/1946/25601/1/PhD-BO-final.pdf.

Oskarsson, N., 1984. Monitoring of fumarole discharge during the 1975–1982 rifting in Krafla volcanic center, North Iceland. J. Volcanol. Geotherm. Res. 22 (1–2), 97–121.

Reynolds, H., Gudmundsson, M.T., Hognadottir, T., Magnusson, E., Palsson, F., 2017. Subglacial volcanic activity above a lateral dyke path during the 2014-2015 Bardarbunga-Holuhraun rifting episode, Iceland. Bull. Volcanol. 79 (6).

Reynolds, H., Gudmundsson, M.T., Hognadottir, T., Palsson, F., 2018. Thermal power of Grimsvotn, Iceland, from 1998 to 2016: Quantifying the effects of volcanic activity and geothermal anomalies. J. Volcanol. Geotherm. Res. 358, 184–193.

Reynolds, H., Gudmundsson, M.T., Hognadottir, T., Axelsson, G., 2019. Changes in Geothermal activity at Bardarbunga, Iceland, following the 2014-2015 Caldera Collapse, Investigated using Geothermal System Modeling. J. Geophys. Res. Solid Earth 124 (8), 8187–8204.

Rooyakkers, S.M., Carroll, K.J., Gutai, A.F., Winpenny, B., Bali, E., Guðfinnsson, G.H., Maclennan, J., Sigmundsson, F., Jónasson, K., Mutch, E.J., 2024. Hydraulically linked reservoirs simultaneously fed the 1975–1984 Krafla fires eruptions: Insights from petrochemistry. Earth Planet. Sci. Lett. 646, 118960.

Sæmundsson, K., 1991. Jardfræði kröflukerfisins. Nátt. Mývatns 662, 24–95 (ISBN 9979906502.).

Sæmundsson, K., 2008a. Krafla. In: Geological Map, 1: 25.000. Landsvirkjun (The National Power Company) and Iceland GeoSurvey.

Sæmundsson, K., 2008b. Krafla. Geothermal Map, 1: 25.000. Landsvirkjun (The National Power Company) and Iceland GeoSurvey.

Sæmundsson, K., Sigurgeirsson, M.Á., Friðleifsson, G.Ó., 2020. Geology and structure of the Reykjanes volcanic system, Iceland. J. Volcanol. Geotherm. Res. 391, 106501.

Scott, S., O'Sullivan, J., Maclaren, O., Nicholson, R., Covell, C., Newson, J., Gudjonsdottir, M., 2022. Bayesian Calibration of a Natural State Geothermal Reservoir Model, Krafla, North Iceland. Water Resour. Res. 58 (2).
SEAN, 1989. In: McClelland, L., Simkin, T., Summers, M., Nielsen, E., Stein, T.C. (Eds.), Global Volcanism 1975–1985. Prentice-Hall, New Jersey, p. 655.
Sigmundsson, F., Vadon, H., Massonnet, D., 1997. Readjustment of the Krafla spreading segment to crustal rifting measured by satellite radar interferometry. Geophys. Res. Lett. 24 (15).
Stimac, J., Goff, F., Goff, C.J., 2015. Intrusion-related geothermal systems. In: The Encyclopedia of Volcanoes. Elsevier, pp. 799–822.
Tryggvason, E., 1984. Widening of the Krafla fissure swarm during the 1975–1981 volcano-tectonic episode. Bull. Volcanol. 47, 47–69.
Turcotte, D.L., Schubert, G., 2014. Geodynamics, 3rd edition. Cambridge University Press. https://doi.org/10.1017/CBO9780511843877.
Violay, M., Gibert, B., Mainprice, D., Evans, B., Dautria, J.M., Azais, P., Pezard, P., 2012. An experimental study of the brittle-ductile transition of basalt at oceanic crust pressure and temperature conditions. J. Geophys. Res. Solid Earth 117 (B3).